Geoscience Data Journal

WILEY

Geoscience Data Journal | RMetS

DATA ARTICLE OPEN ACCESS

High-Resolution Digital Terrain Model and Land-Surface Parameters of São Sebastião and Ilhabela, Southeastern Brazil

Rebeca Durço Coelho[1,2] | Gabriella Labate Frugis[2,3] | Camila Duelis Viana[1,2] | Carlos Henrique Grohmann[2,3]

[1]Institute of Geosciences, Universidade de São Paulo, São Paulo, Brazil | [2]Spatial Analysis and Modelling Lab, SPAMLab, IAG-USP, São Paulo, Brazil | [3]Institute of Astronomy, Geophysics and Atmospheric Sciences, Universidade de São Paulo, São Paulo, Brazil

Correspondence: Carlos Henrique Grohmann (guano@usp.br)

Received: 11 September 2025 | **Revised:** 3 January 2026 | **Accepted:** 8 January 2026

Keywords: geomorphology | geomorphometry | landslide | lidar | tectonics | territorial planning

ABSTRACT

Effective disaster risk management and detailed environmental studies in landslide-prone regions require high-resolution and accurate Digital Terrain Models (DTMs). This work describes the development of a 2 m-resolution lidar-based DTM and an extensive set of land-surface parameters (LSPs) for the municipalities of São Sebastião and Ilhabela, southeastern Brazil. The dataset was generated from approximately 650 GB of airborne lidar point clouds, processed through a reproducible workflow comprising ground point classification, merging of filtered files, Triangulated Irregular Network (TIN) interpolation, gap filling and surface smoothing. The resulting high spatial resolution enabled the extraction of topographic parameters for local-scale landslide susceptibility analyses, surpassing the detail of existing photogrammetric and global DEMs for the region, revealing geomorphological features previously indiscernible, including past landslide deposits, drainage captures and structural lineaments. The resulting products represent the first openly accessible high-resolution DTM for this region, made available via Zenodo, thus supporting applications in landslide susceptibility mapping, environmental modelling and territorial planning. This open-access initiative contributes to bridging the gap in Brazil's high-resolution topographic data availability and fosters both scientific research and evidence-based decision-making.

1 | Introduction

Digital Elevation Models (DEMs) are ubiquitous datasets in science to represent Earth's surface. More specifically, a Digital Surface Model (DSM) marks the lower boundary of the atmosphere (with the terrain, water bodies, ice, vegetation or human-made objects), while a Digital Terrain Model (DTM) records the boundary between the terrain (lithosphere) and the atmosphere, without vegetation, buildings etc., also being called a "bare-earth" DEM (Guth et al. 2021).

DEMs can be generated by various means such as InSAR (Interferometric Synthetic Aperture Radar), photogrammetry of optical imagery and lidar (light detection and ranging), with terrestrial, airborne or spaceborne sensors (Nelson et al. 2009). Photogrammetry always produces DSMs, since optical images cannot provide information below the canopy (Winsen and Hamilton 2023). InSAR can produce DSMs or DTMs, depending on the wavelength employed; longer wavelengths may penetrate foliage, but shorter wavelengths will be reflected at the top or mid-canopy. Time of data acquisition will also

Rebeca Durço Coelho and Gabriella Labate Frugis are co-first authors.

influence the results due to loss of foliage in temperate forests during autumn (allowing more signal penetration even with shorter wavelengths) or snow coverage in winter (Carabajal and Harding 2006). Lidar can also produce DSMs or DTMs, as the sensors can register several reflections of the same emitted laser pulse, from the top of the canopy to intermediate objects, through the ground (Fowler et al. 2007).

There are several global (or quasi-global) DEMs available at no cost to the user, such as SRTM (Shuttle Radar Topography Mission—Farr et al. 2007), ASTER GDEM (ASTER Global DEM—Tachikawa et al. 2011), ALOS AW3D30 (ALOS World 3D—Tadono et al. 2015), NASADEM (Crippen et al. 2016) and Copernicus DEM (CopDEM—Strobl 2020), all distributed at a resolution of 1 arc-second (~30 m at the Equator). These are all considered as DSMs due to their methods of generation (InSAR for SRTM and Copernicus DEM, photogrammetry for ALOS AW3D30 and ASTER GDEM), although SRTM and CopDEM show elevations closer to mid-canopy in some regions (Carabajal and Harding 2006; Guth and Geoffroy 2021).

Recently, several endeavours have been presented to create DTMs with machine learning methods, based on the global DSMs and ancillary data (local lidar data, land-use maps, etc.). These 'edited DEMs' include FABDEM (Hawker et al. 2022), FathomDEM (Uhe et al. 2025) and GEDTM (Ho et al. 2025) with full global coverage, DeltaDTM (Pronk et al. 2024) and DiluviumDEM (Dusseau et al. 2023), which focus on coastal areas, and ANADEM (Laipelt et al. 2024) covering South America. The DEMIX Initiative (Strobl et al. 2021) carried out extensive comparisons of these DEMs and ranks CopDEM as the best global DSM, noting that SRTM, NASADEM and ASTGER GDEM should be considered legacy datasets (Bielski et al. 2024; Guth et al. 2024).

Country-wide DEMs are commonly based on lidar or photogrammetry of high-resolution orbital or airborne imagery. Examples include the USGS 3D Elevation Program (3DEP), which provides a lidar-based multi-resolution dataset at resolutions of approximately 30, 10 and 3 m for the conterminous United States and at 1 m for parts of the United States;[1] most European countries offer open access to lidar-based DEMs, as well as New Zealand; Mexico has 1 and 5 m lidar DEMs for several areas of the country.

Brazil is a country of continental dimensions, but lacks detailed topographic mapping of its territory. Currently, the Federal agency responsible for systematic mapping, IBGE (*Instituto Brasileiro de Geografia e Estatística*—Brazilian Institute for Geography and Statistics), indicates that 100% of the territory is mapped at a 1:250,000 scale, 70% at a 1:100,000, 15% at a 1:50,000, and only 1% at 1:25,000.[2]

In the 2010s, a joint initiative of the Brazilian Army and Air Force sought to fill the Amazonian 'cartographic void' (areas with mapping at 1:250,000 or less) with airborne InSAR in a project known as 'Radiography of Amazonia' (RAM) (Grohmann 2015). The resulting available data are 5 m DSMs distributed under a restrictive licence (the data are considered sensitive and cannot be shared with foreign researchers, for example) through the Army's Geoportal.[3] Initially, there was also availability of DTMs and raw radar images, but that data is now for exclusive use of the Brazilian Armed Forces.

In Brazil, each state is responsible for topographic mapping at scales of 1:10,000 or larger. While some states have traditional maps with such level of detail, others are investing in lidar and/or photogrammetric surveys to update their geospatial databases. Photogrammetric DEMs with a resolution of 2 m are available for the states of Espírito Santo[4] and Santa Catarina,[5] while Bahia[6] and Amapá[7] have partial state coverage of 5 m DEMs from airborne InSAR (the same system used by the RAM project).

São Paulo offers 5 m DSM and DTM for the whole state, although these are interpolated from photogrammetrically-derived point heights with 15 m spacing, and present numerous issues, such as interpolation artefacts and surface texture mismatch between adjacent tiles. Pernambuco was the first state to provide open DSMs and DTMs from lidar surveys,[8] with 1 m resolution (Cirilo et al. 2014). Most of the state capitals (and other large cities) have lidar surveys, but do not distribute the data due to a lack of digital infrastructure to host and serve large amounts of data. The city of São Paulo, the most populous city in the country (and fourth in the world, with ~11,450,000 inhabitants), serves two lidar surveys (2017 and 2020) through the city's geoportal, GeoSampa.[9] The data is distributed as point clouds in LAS format. Grohmann and Gomes (2022) created a DSM and a DTM from the 2017 data and hosted them on Kaggle.

The Geographical and Cartographic Institute of São Paulo (IGC-SP—*Instituto Geográfico e Cartográfico do Estado de São Paulo*) the official cartographic agency of the São Paulo State coordinate a project to map the entire state area with lidar. The surveys happened between 2023 and 2024. The point clouds have a minimum point density of 10 pts/m^2 in the Metropolitan Region of São Paulo (the city of São Paulo and its neighbouring cities) and of 4 pts/m^2 in the rest of the state.

In the night of 18–19th February 2023, a massive rainfall event struck the northern shore of São Paulo State (Figure 1A). In the city of São Sebastião, a precipitation of more than 600 mm in 24 h led to widespread landslides, floods and localised debris flows, causing 65 casualties and major infrastructure damage; in the neighbouring Ilhabela, the rainfall reached 337 mm and affected mainly its southern region, triggering landslides detectable in aerial imagery on more elevated hillsides (Marengo et al. 2024).

Several inventories of these landslides have been created, using different methods and data. Marengo et al. (2024) used PlanetLabs imagery at 3 m resolution to map landslide scars, debris flows, landslide deposits, debris fans and mud deposits, reporting a total area of almost 2×10^6 m^2. Coelho et al. (2024) produced an inventory of the landslides scars (Figure 1B) based on a 10 cm resolution orthomosaic released by the São Paulo State Government only a few days after the disaster (Figure 1C). The inventory contains 1070 landslide scar polygons and is openly available in Zenodo. Bonini et al. (2025) created a landslide inventory for the same area using an object-based Random Forest approach, identifying 396 scars in São Sebastião and 100

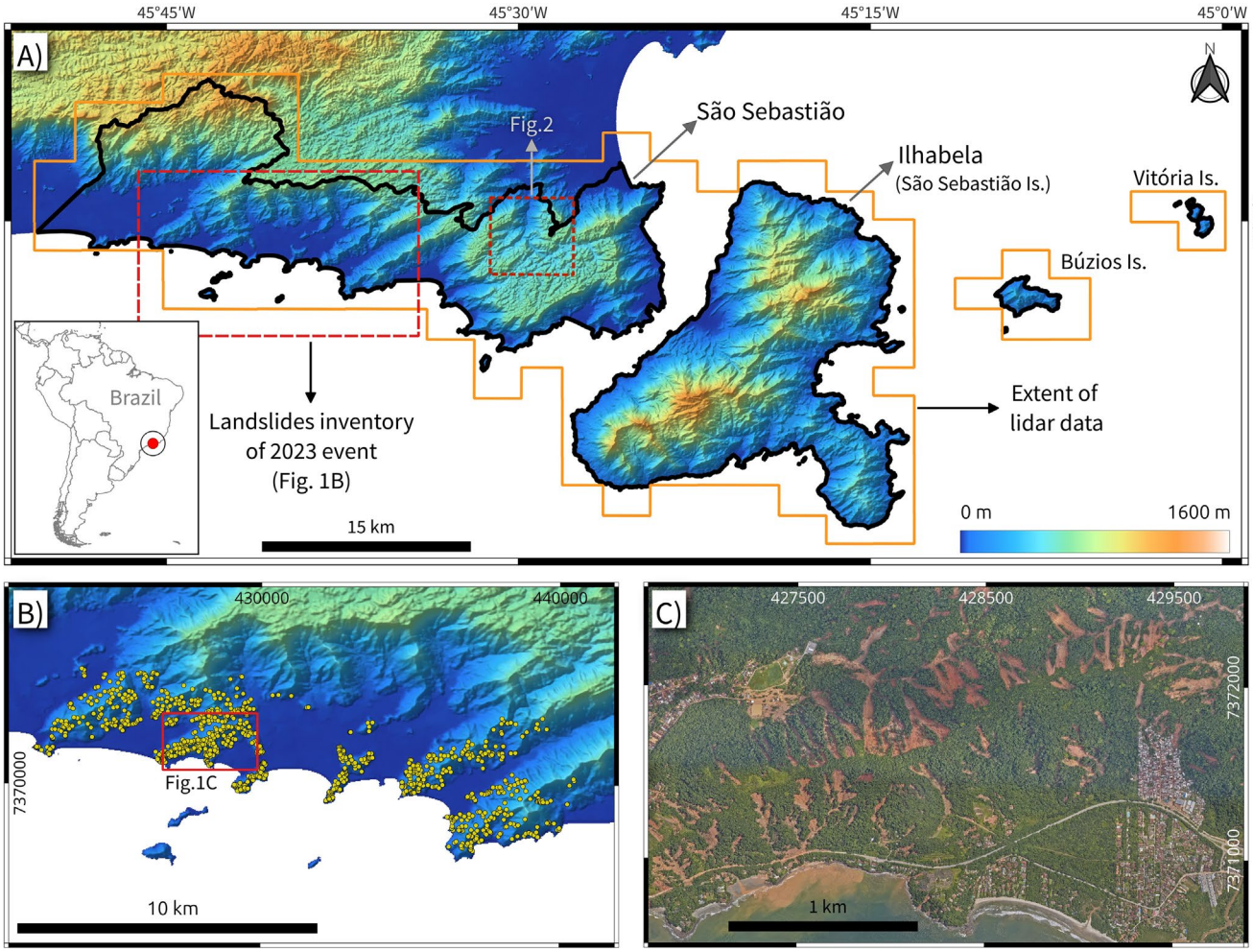

FIGURE 1 | (A) Location and morphological context of São Sebastião and Ilhabela municipalities, southeastern Brazil. The thick black line marks the cities' boundaries. Orange line show the limits of lidar data. Terrain morphology from FABDEM (Hawker et al. 2022). Insets (red dashed line), delimits the area of the landslides inventory by Coelho et al. (2024) (shown in B) and of Figure 5. (B) Landslide inventory for the 2023 event (Coelho et al. 2024). (C) Orthophoto of the landslides, surveyed on 25 February 2023 by the São Paulo State Government (IDE-SP 2023).

in Ilhabela. We do note that both Marengo et al. (2024) and Bonini et al. (2025) state that their datasets are available upon request, a practice considered inefficient in terms of data sharing by Tedersoo et al. (2021).

Efforts to prevent future disasters in the region include improving landslide susceptibility maps for the area. Landslide susceptibility analysis intends to recognise the conditions in which past landslides occurred, and employ that information to determine where new events might happen (Aleotti and Chowdhury 1999; Guzzetti et al. 2012). A review of such studies in Brazil by Dias et al. (2021) revealed that DEMs are widely used to derive land-surface parameters (LSPs—slope, aspect, curvatures, etc.) used as input for susceptibility models. Given the scarcity of high-resolution open elevation data in Brazil, researchers resort to global DEMs like SRTM or CopDEM. For example, Varnier (2024) used NASADEM and Random Forest within Google Earth Engine to evaluate landslide susceptibility for the municipalities of São Sebastião and Ilhabela, mapping 5.4% of the area as highly susceptible. Alcântara et al. (2024) used a weighted sum model to develop susceptibility maps for four climate scenarios from the Intergovernmental Panel on Climate Change (IPCC), but did not specify the source of the elevation data.

While the resolution of ~30 m might be enough for regional-scale analysis, it lacks the angular coherence between neighbouring pixels necessary to derive LSPs for detailed studies (Hengl 2006; Valeriano et al. 2006; Grohmann et al. 2007). Moreover, each pixel represents an area of ~900 m^2, which can be larger than entire small landslides.

To properly study landslide susceptibility on a local scale, lidar data are the best option. If data are acquired before a landslide event, DTMs with 1–5 m resolution can faithfully represent the topography and derived LSPs. In the case of post-event surveys, one can calculate the difference between the DSM and the DTM to highlight the scars and deposit areas.

After negotiations with the IGC-SP, our research group obtained access to the raw lidar data for São Sebastião and Ilhabela in order to produce landslide susceptibility maps based on a high-resolution DTM and to provide technical feedback to IGC-SP on the quality of the data. Although raw data cannot be shared,

derivative products such as DEMs and LSPs can. Therefore, following the principles of Open Science (OECD 2015), in this paper we describe a high-resolution dataset of elevation and land-surface parameters derived from the lidar data. We understand these data are invaluable not only to academic researchers studying the region but also to policymakers and the Public Administration.

2 | Data and Methods

The data used in this study consist of raw airborne lidar point cloud files in LAS format, totaling approximately 650 GB of data. The data cover the entire area of the municipalities of São Sebastião and Ilhabela (Figure 1).

The LAS files follow the ASPRS LAS 1.4 specification (ASPRS 2011) and include standard point attributes such as XYZ coordinates, intensity, return number, number of returns, classification and GPS time. All data are provided in the WGS84/UTM zone 23S coordinate reference system (EPSG:32723), with altimetric information converted to Normal (H^N) using the `hgeoHNOR2020` model provided by IBGE (2023). Point classification encompasses ground, low/medium/high vegetation and buildings. The ground point density varies across acquisition blocks, with an average of 0.32 points per square metre, ensuring sufficient detail to generate digital terrain models with a grid spacing of 2 m (Anderson et al. 2006; Hengl 2006).

All data processing and analysis steps were performed using a combination of open-source and proprietary tools. Specifically, we employed WhiteboxTools[10] (WbT) and Whitebox Workflows[11] (WbW) libraries (J. Lindsay 2016) for lidar data processing and terrain analysis. The task 'smooth vegetation residual' was performed using Whitebox Workflows Professional, the commercial version of the Whitebox suite, which offers extended functionality for point cloud manipulation and surface modelling.

2.1 | Lidar Data Processing and DTM Generation

The lidar data processing workflow consisted of five main stages: ground point filtering, merging of filtered files, DTM generation via TIN interpolation, gap filling in the DTM and subsequent surface smoothing (Table 1). All raster outputs at each stage were exported in compressed TIFF format to optimise storage and ensure compatibility with subsequent analyses. Throughout the workflow, file/object existence checks and systematic memory management were applied to enhance computational efficiency and guarantee reproducibility.

When examining the point cloud classification for the small islands and the shoreline of the main island of the Ilhabela Archipelago, discrepancies were found between the assigned classes and the actual surface conditions (Figure 2). In several rocky areas with no vegetation cover, no ground-classified points were present. A similar issue occurred in the interior of the smaller islands, despite their vegetation density being comparable to that of the main island, where the classification appeared correct.

In these problematic regions, a large number of points had been classified as water, even though they clearly corresponded to land. An inspection in CloudCompare (Girardeau-Montaut 2019) confirmed that these water-classified points were in fact ground points. The most likely cause is that, in areas close to the sea, the classification algorithm failed to correctly distinguish the land-water boundary.

To address this issue, we delineated the coastlines of the smaller islands and applied a shoreline buffer around the main island. The original point cloud files were then clipped to these polygons, and the `filter_lidar` tool (WbW Pro) was applied to retain the last and single returns of water-classified points, thereby correcting the classification error in these coastal areas. Using the `lidar_join` tool, these filtered points were merged with the ground-classified points previously filtered.

TABLE 1 | Whitebox tools and parameters for each step of the lidar processing workflow applied to the DTM generation.

Step	Description	WbW tool	Main parameters
Step 1	Ground point filtering	`filter_lidar_classes` or `filter_lidar` (WbW Pro)	exclusion_classes = [1, 3–19]
Step 2	Merging filtered LAS files	`lidar_join`	Region-specific files merged
Step 3	TIN interpolation	`lidar_tin_gridding`	cell_size = 2 m, max_triangle_edge = 1000 m
Step 4	Filling DTM gaps	`fill_missing_data`	filter_size = 51, weight = 2.0, exclude edges
Step 5a	Remove off-terrain objects (J. B. Lindsay 2018)	`remove_off_terrain_objects`	filter_size = 7, slope_threshold = 11.0
Step 5b	Smooth vegetation residual (WbW Pro)	`smooth_vegetation_residual`	max_scale = 15, dev_threshold = 0.06, scale_threshold = 4 (2 passes)
Step 5c	Feature-preserving smoothing (Lindsay, Francioni, and Cockburn 2019)	`feature_preserving_smoothing`	filter_size = 3, normal_diff_threshold = 12.0, iterations = 1

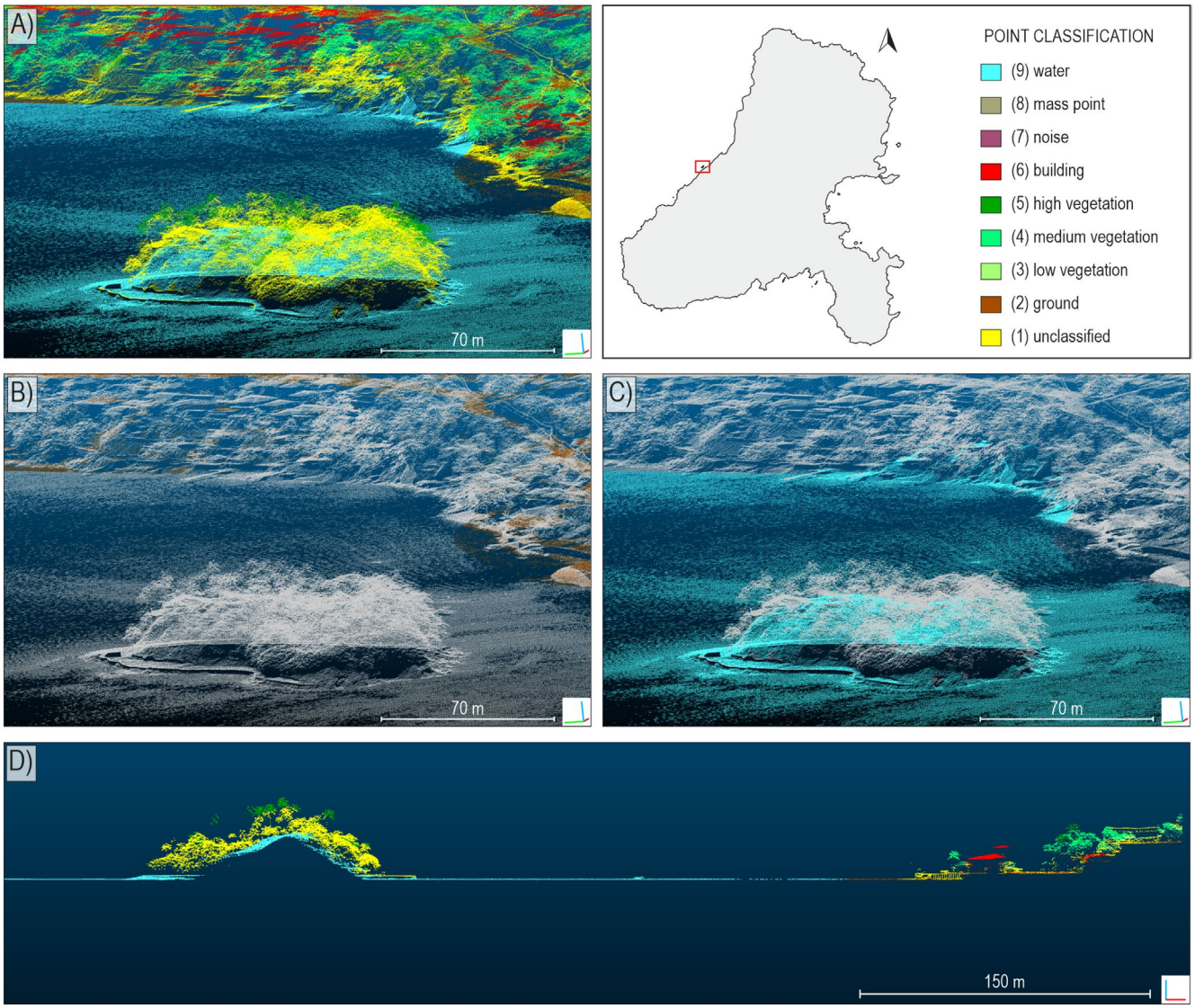

FIGURE 2 | Perspective view of the Ilha das Cabras point cloud (Ilhabela), showing the misclassification along land-water boundaries. (A) All classes. (B) Ground-classified points in orange-brown. (C) Water-classified points in cyan. (D) Cross-section view showing water-classified points extending over the land area of Ilha das Cabras.

2.2 | DTM Altimetric Assessment

The study area's rugged topography, characterised by steep escarpments and dense Atlantic Forest cover, imposes severe logistical constraints on geodetic infrastructure. Consequently, the regional geodetic network is sparse, comprising only five active stations (Figure 3), which were not used in the altimetric assessment. Data and metadata for the IBGE stations can be accessed through the Brazilian Geodetic Database (BDG–IBGE).[12] As an alternative, elevation control points were extracted from 1:10,000 scale topographic maps produced by IGC-SP. Even though these maps were produced in the 1970s, they are the most detailed topographic information published for the study area.

This reliance on historical mapping introduces a significant methodological challenge: the 1970s cartography, while compliant with its era's standards, lacks the vertical precision of modern active sensors. Therefore, this analysis is framed not as an absolute validation, but as a *cross-comparison assessment* to quantify the consistency between the lidar-derived DTM and the available cartographic records.

These maps are currently distributed through the São Paulo State Spatial Data Infrastructure (IDE-SP)[13] and were accessed via Web Map Service (WMS) protocol in QGIS.

After loading the topographic maps via WMS, 30 spot height points were selected within the spatial extent of each DTM—approximately 524 km^2 for São Sebastião and 347 km^2 for Ilhabela (Figure 3 and Supporting Information). Priority was given to locations on forested hilltops and stable natural slopes, to ensure spatial representativeness while accounting for the region's predominant land cover (> 80%). This sampling size follows the base recommendations for project areas ≤ 1000 km^2 according to Table C.1 of the ASPRS 2024 standards (ASPRS 2024).

Given the extreme accessibility constraints, these 30 points serve as a hybrid sample to characterise discrepancies in both

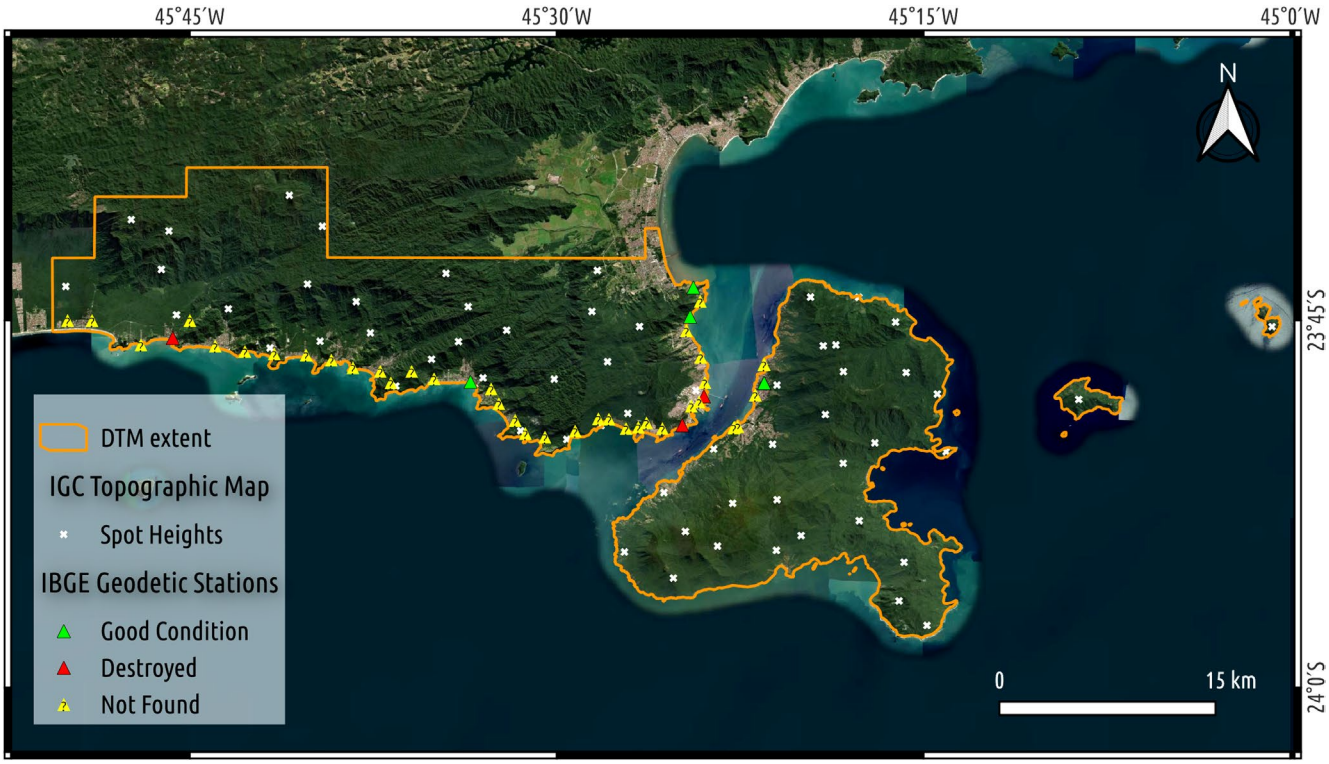

FIGURE 3 | DTM extent and spatial distribution of elevation reference points and IBGE geodetic stations. White crosses represent the IGC topographic spot heights (1:10,000 scale) used for DTM assessment. Triangles indicate IBGE geodetic stations. Background: Esri 'World Imagery'.

non-vegetated and vegetated environments, traditionally referred to as Non-vegetated (NVA) and Vegetated Vertical Accuracy (VVA). Furthermore, the results must be interpreted within the context of the ~50 years gap between the original photogrammetric restitution and the lidar acquisition. Geomorphological processes, erosion and land-use changes during this interval, coupled with the inherent limitations of airborne photogrammetry in dense canopy, contribute to the observed residuals.

The vertical discrepancy, hereafter referred to as the *Vertical Residual* (R_v), was calculated by subtracting the 1978 topographic elevation from the lidar-derived elevation:

$$R_v = \text{Elevation}_{\text{lidar}} - \text{Elevation}_{\text{IGC}} \quad (1)$$

where $\text{Elevation}_{\text{lidar}}$ represents the orthometric height from the 2-m lidar-derived DTM and $\text{Elevation}_{\text{IGC}}$ corresponds to the spot heights extracted from the IGC topographic maps.

The vertical consistency of each model was subsequently quantified using the root mean square error (RMSE—Equation 2), mean error (Bias—Equation 3) and the standard deviation (σ—Equation 4) of the residuals:

$$\text{RMSE} = \sqrt{\frac{1}{n}\sum_{i=1}^{n} R_{v,i}^2} \quad (2)$$

$$\text{Bias} = \overline{R}_v = \frac{1}{n}\sum_{i=1}^{n} R_{v,i} \quad (3)$$

$$\sigma = \sqrt{\frac{1}{n}\sum_{i=1}^{n}\left(R_{v,i} - \overline{R}_v\right)^2} \quad (4)$$

where n is the number of reference points, and $R_{v,i}$ is the vertical residual for each point.

It is essential to emphasise that R_v is a composite metric. It incorporates the propagated uncertainty from three primary sources: (i) the intrinsic precision of the lidar-derived DTM; (ii) the nominal accuracy of the 1:10,000 scale topographic maps; and (iii) the environmental changes occurred since the 1970s. Conceptually, this residual does not represent an absolute measurement of sensor error, but rather a *methodological discrepancy*.

Statistical results (Table 2) show RMSE values of 2.55 m for São Sebastião and 2.44 m for Ilhabela, classifying the models within the 300-cm Vertical Accuracy Class according to ASPRS (2024) standards. The consistent negative bias (−1.61 and −1.89 m) indicates that the lidar elevations are lower than those found in the 1:10,000 topographic reference. This trend is attributed to the lidar's capability to penetrate the forest canopy and reach the terrain surface, whereas the 1978 photogrammetric mapping likely registered an intermediate position between the ground and the top of canopy in these densely forested areas.

In these steep and forested areas, the 1978 photogrammetric restitution was limited by the inability of passive sensors to penetrate dense foliage. The negative residuals observed here represent the successful removal of this 'vegetation noise' by

the lidar pulses. Thus, the observed discrepancies are primarily attributed to the transition from manual, vegetation-influenced restitution to high-resolution active remote sensing rather than intrinsic sensor failure.

TABLE 2 | Vertical accuracy metrics for DTM assessment.

	Dependent variable: Vertical residual (R_v)				
Area	**Bias (m)**	**RMSE (m)**	**SD (σ) (m)**	**Min (m)**	**Max (m)**
São Sebastião	−1.61	2.55	2.02	−4.87	0.83
Ilhabela	−1.89	2.44	1.57	4.89	1.61
Check points (n)	60 (30 per area)				
Reference scale	1:10,000 (IGC topographic maps)				
Vertical datum	Imbituba (SGB)				

This interpretation is visually confirmed by the distribution of residuals (Figure 4). The histograms and boxplots reveal that the error mass is consistently shifted below the zero-baseline, while the scatter plot shows the 2 m-DTM elevations following the 1:1 identity line with a constant downward offset. As per ASPRS (2024) guidelines, diagnosing such systematic offsets is critical for data transparency and for the legitimate use of pre-existing cartography as a baseline for modern geoscientific modelling.

2.3 | Land-Surface Parameters and Objects

Land-surface parameters (LSPs) and land-surface objects (LSOs) are the two DEM-derived entities fundamental to modern geomorphometry (Mark and Smith 2004; Pike et al. 2009). An LSP is a descriptive and quantitative measure of surface characteristics, such as slope, aspect and curvatures. An LSO is a discrete spatial feature, such as a drainage network, ridge or watershed lines. We provide a set of 17 LSPs and LSOs that comprise several facets of the landscape, including illumination, shape, landform characteristics and hydrology.

Figure 5 shows an example of three LSPs (hillshade, slope and surface roughness) for the 2 m lidar DTM (Figure 5A–C), a 5 m

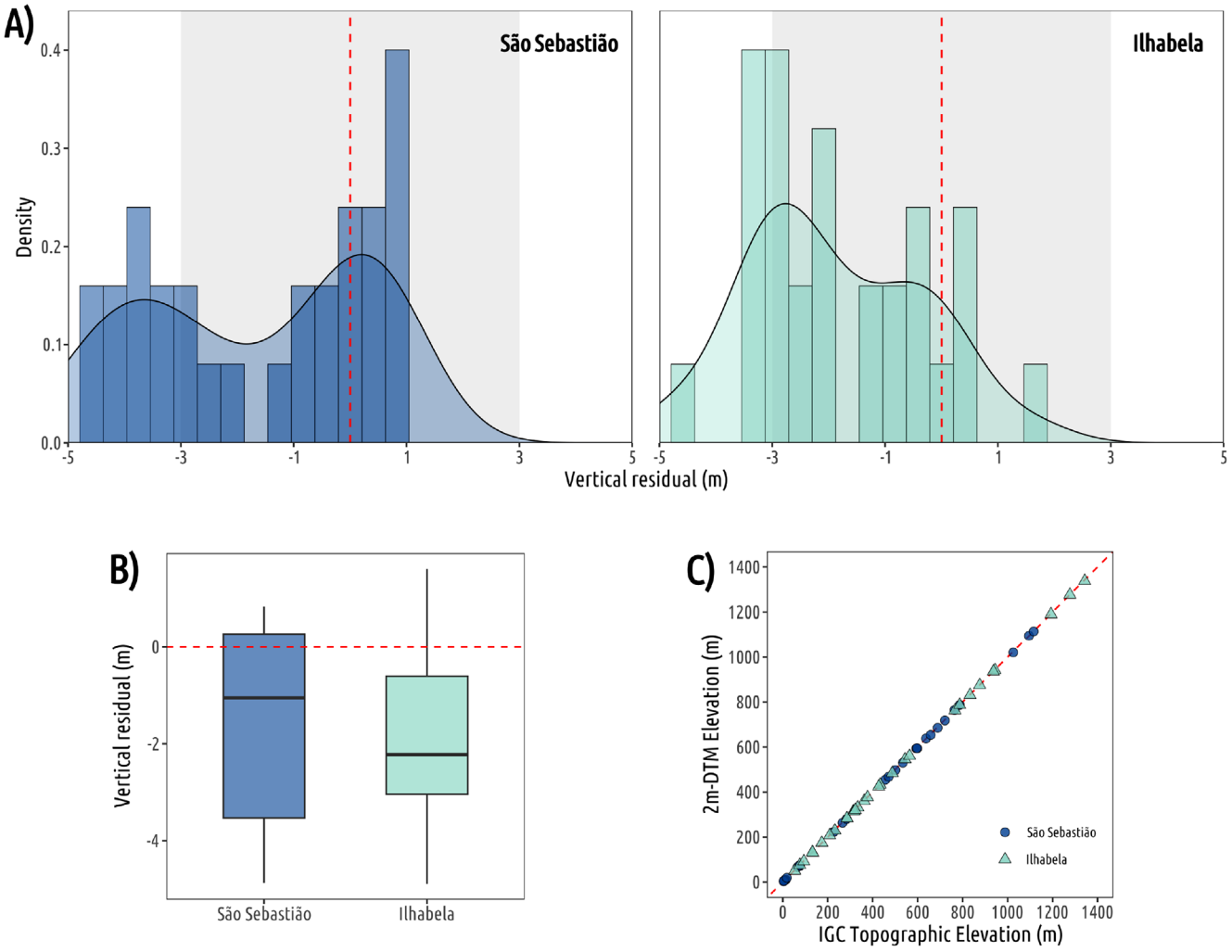

FIGURE 4 | Vertical accuracy assessment of the 2 m-DTM. (A) Density distribution of residuals (R_v); (B) Boxplot showing the dispersion of vertical residuals; (C) Correlation between Elevation_{IGC} and Elevation_{lidar}.

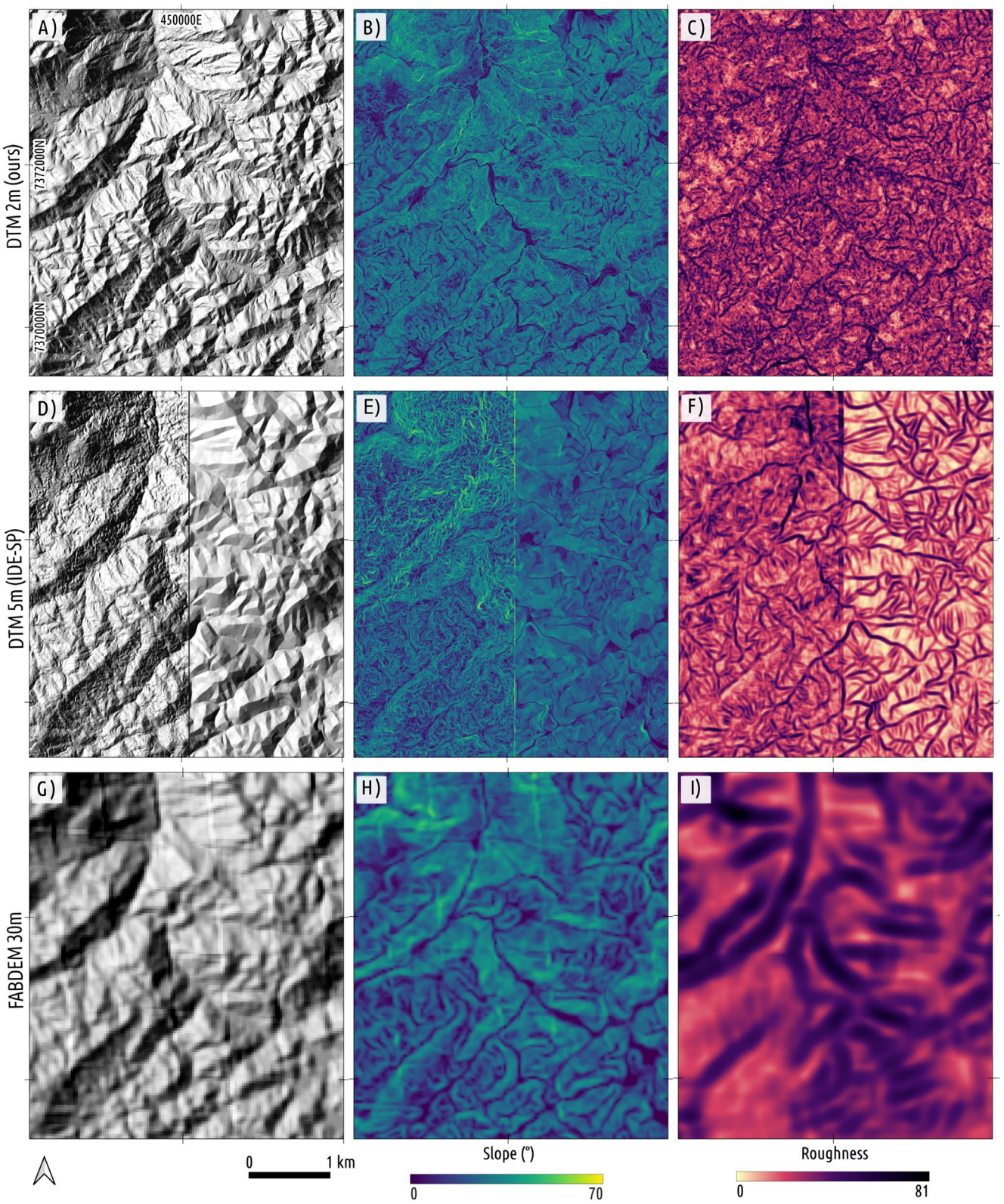

FIGURE 5 | Comparison of terrain parameters derived from high-resolution (DTM 2 m), intermediate resolution (DTM 5 m from IDE-SP), and coarse resolution (FABDEM 30 m) DEMs for the study area. Location of area shown in Figure 1. (A, D, G) Hillshade. (B, E, H) Slope. (C, F, I) Surface roughness.

photogrammetric DTM from IDE-SP (Figure 5D–F), and the 30 m FABDEM DTM (Figure 5G–I). The area is almost completely covered by dense forests and was selected to illustrate not only the effectiveness of our processing workflow, providing a clean surface while preserving the sharpness of ridgelines, but also some issues with the other datasets. The 5 m DTM has a clear north–south division in two areas with contrasting texture, indicating poor vegetation filtering. FABDEM shows an

issue often overlooked by DEM users: linear artefacts caused by cell size adjustment due to projection from Lat-Long to UTM (Grohmann and Steiner 2008).

Hillshade, or shaded relief, is a technique of terrain visualization considering the orientation of a light source and the local slope and aspect (Horn 1981; Imhof 1982). We used the tool `multidirectional_hillshade` and set altitude to 30° and Z-factor to 1 as default.

Slope steepness was calculated with the `slope` tool, with the output in degrees. Since the data are in a projected coordinate system, this tool uses a polynomial fit of the elevations within the 5×5 neighbourhood surrounding each cell (Florinsky 2016).

Aspect, the slope orientation in degrees clockwise from north, was calculated with the `aspect` tool, using a 5×5 neighbourhood of each cell (Florinsky 2016).

Profile curvature is the rate of change in slope along a flow line, and characterises the degree of downslope acceleration or deceleration (Gallant and Wilson 2000). Profile curvature is negative for slope increasing downhill (convex) and positive for slope decreasing downhill (concave). We used the tool `profile_curvature`, with output in units of m^{-1}.

Plan curvature (or contour curvature), is the rate of change in aspect along a contour line, and characterises the degree of flow convergence or divergence within the landscape (Gallant and Wilson 2000). Plan curvature is negative for diverging flow and positive for convergent areas. We used the tool `plan_curvature`, with output in units of m^{-1}.

Minimal curvature is the curvature of a principal section with the lowest value of curvature at a given point of the topography (Florinsky 2017). Positive values correspond to hills while negative values correspond to valley positions (Florinsky 2016). We used the tool `minimal_curvature`, with output in units of m^{-1}, and set the `log_transform` option to `True`.

Maximal curvature is the curvature of a principal section with the highest value of curvature at a given point of the topography (Florinsky 2017). Positive values correspond to ridges while negative values indicate closed depressions (Florinsky 2016). We used the tool `maximal_curvature`, with output in units of m^{-1}, and set the `log_transform` option to `True`.

Difference from mean elevation is the difference between the elevation of each grid cell and the mean elevation of its local neighbourhood, being a measurement of relative topographic position. We used the tool `difference_from_mean_elevation`, and set `filterx` and `filterx` to 11 grid cells.

Shape index (Koenderink and van Doorn 1992) is a dimensionless variable ranging from −1 to 1, useful for landform classification. Positive values indicate convex landforms, and negative values correspond to concave landforms (Florinsky 2017). Absolute values from 0.0 to 0.5 are characteristic of hyperbolic forms (saddles), while absolute values from 0.5 to 1.0 are associated with elliptic forms (hills and closed depressions). We used the tool `shape_index`, which requires a licence for Whitebox Workflows for Python Professional.

The *Geomorphons* landform classification is based on a line-of-sight analysis for the eight topographic profiles in the cardinal directions surrounding each grid cell of the input DEM (Jasiewicz and Stepinski 2013). We used the `geomorphons` tool with default parameters.

Spherical standard deviation of normals measures the angular dispersion of the surface normal vectors within a local neighbourhood, being a measure of *surface roughness*, complexity and texture (Grohmann et al. 2011; Lindsay, Newman, and Francioni 2019). We used the tool `spherical_std_dev_of_normals`, and set `filter_size` to 11 grid cells.

Flow accumulation was calculated with the multiple-flow-direction (MFD) algorithm from Qin et al. (2007). The DTM was pre-processed with the `breach_depressions_least_cost` tool (Lindsay and Dhun 2015) with the `max_dist` set to 900 m. We then used the `qin_flow_accumulation` tool, with `out_type` set to `sca` (specific contributing area—the catchment area divided by the flow width), and `log_transform` set to `False`.

Wetness index describes the tendency for a site to be saturated to the surface, given its contributing area and local slope characteristics. This raster was calculated with the `wetness_index` tool, using the flow accumulation and slope rasters as inputs.

Flow direction is commonly used as input for other spatial hydrology and stream network analysis. In the Whitebox suite, this is calculated with the `d8_pointer` tool, which is based on the D8 algorithm (O'Callaghan and Mark 1984).

A *Stream network* can be derived from a DEM based on a flow accumulation raster and a specified threshold, which represents the minimum area required to initiate and maintain a channel. We used the `extract_streams` tool with the flow accumulation raster as input and the `threshold` set to 4000 for São Sebastião and 1500 for Ilhabela.

3 | Topographic Features of Interest

Upon inspection of the DTM and derived LSPs, several interesting topographic features were identified, including evidence of past large landslide deposits, river captures and subvolcanic landforms. A selection of examples is shown in Figure 6.

Past landslide indications are highlighted in profile curvature maps by convex and concave landform patterns. Figure 6A shows colluvial deposits from past landslides just north of Vila Sahy, an area heavily affected by the event of 2023. A relic landslide scarp is visible in Figure 6D, to the west of Castelhanos Beach in Ilhabela.

A drainage capture is shown in Figure 6B, where a small drainage bends abruptly (indicated by a white arrow) before flowing

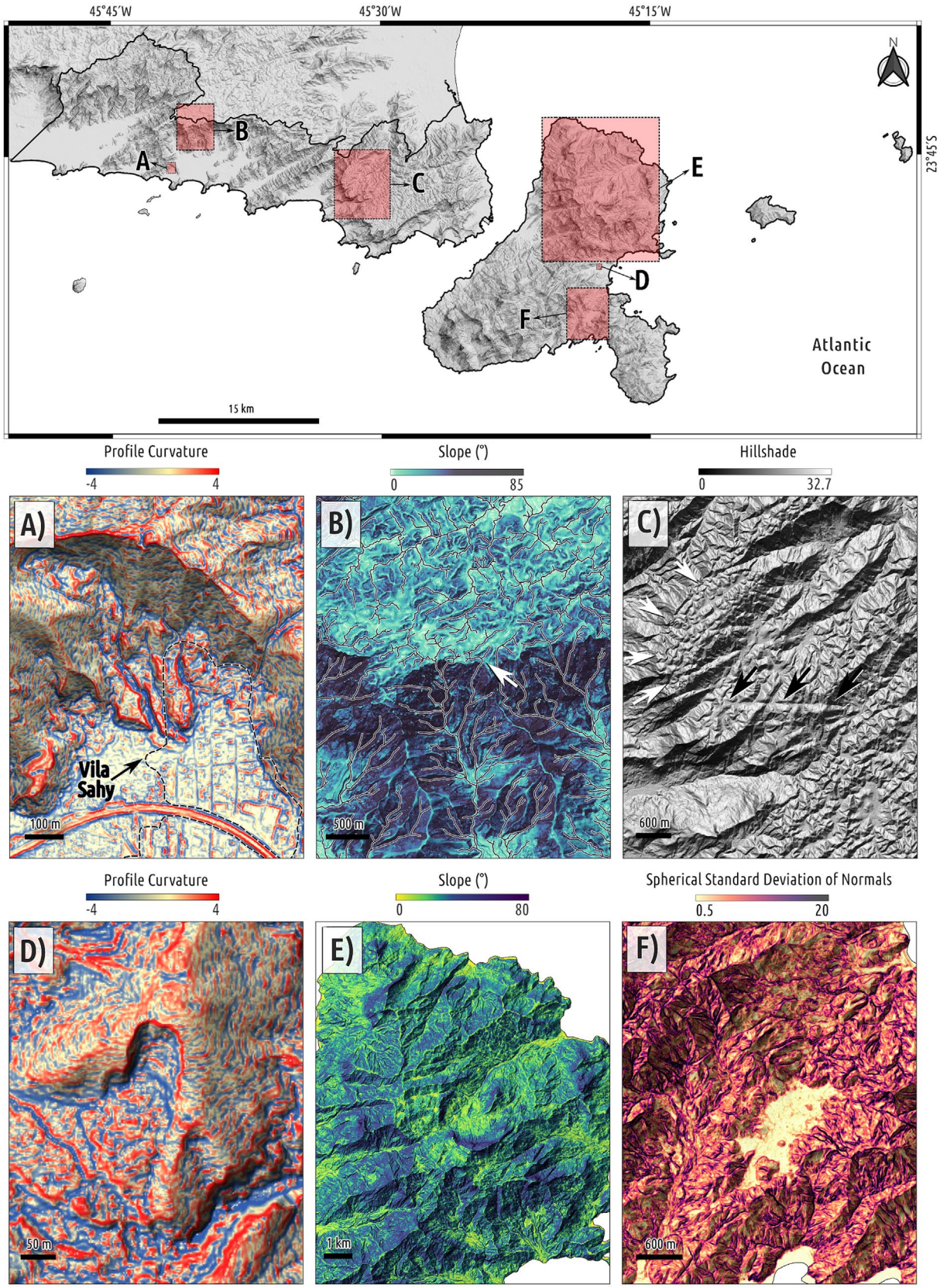

FIGURE 6 | Examples of relevant topographic features identified within the study area, based on different terrain variables derived from the Digital Terrain Model (DTM). (A) Deposits of past landslides in the Vila Sahy region, highlighted by convex and concave landform patterns; (B) Drainage capture at the transition between the plateau and the escarpment (indicated by the white arrow); (C) Structural lineaments revealed by variations in terrain illumination (black and white arrows); (D) Scarp of a past landslide with a prominent colluvial deposit downslope; (E) Concentric circular ridges, associated with subvolcanic alkaline plutonism; (F) Flat-bottom depression evidenced by low surface roughness compared to the surrounding area.

south from the plateau. Over the plateau, a trellis drainage pattern is observed, indicating a structural control over the stream network. Large tectonic lineaments are seen in Figure 6C: an E-W lineament is marked by black arrows, and a curvilinear structure is indicated by white arrows.

In Figure 6E, the slope map highlights concentric circular ridges of the Serraria Stock, which is part of the 88–85 Ma alkaline plutonic event of the Serra do Mar Province (Sato 2006; Sato et al. 2008; Giraldo-Arroyave et al. 2021). In Figure 6F, a flat-bottomed depression is visible in a surface roughness map, just north of Indaiaúba Beach; this depression is not clearly identifiable in optical imagery due to dense forest cover.

4 | Conclusions

This study presents the first publicly available high-resolution Digital Terrain Model (i.e., 'bare-earth') and a comprehensive set of land-surface parameters (LSPs) for the municipalities of São Sebastião and Ilhabela, southeastern Brazil, derived from airborne lidar data. The 2 m-resolution DTM significantly enhances the representation of topographic features when compared to existing regional and global elevation datasets, allowing the identification of subtle geomorphological structures relevant to landslide susceptibility assessment and environmental studies. By providing an open-access dataset processed with a transparent and reproducible workflow, this work contributes to filling a critical gap in Brazil's high-resolution topographic data availability, promoting applications that range from scientific research to disaster risk management and territorial planning. Future work should explore the integration of this dataset with multitemporal remote sensing products and climate projections to refine hazard models and support adaptive strategies in vulnerable mountainous regions.

Acknowledgements

This project was supported by The São Paulo Research Foundation (FAPESP—grant #2023/11197-1) and CNPq (grants #300033/2025-7, #311209/2021-1). R.D.C. is a PhD student financed by the Brazilian Federal Agency for Support and Evaluation of Graduate Education (CAPES—Finance Code 001). G.L.F. is a post-doc researcher financed by CAPES PIPD (grant 88887.122984/2025-00). We are thankful to John B. Lindsay (Guelph University) for providing a licence of Whitebox Tools Pro and for assistance in lidar data processing. Raw lidar data was kindly provided by the Geographical and Cartographic Institute of São Paulo, under a data transfer agreement with C.H.G: *Base cartográfica: Nuvem de Pontos LiDAR 2023/2024, 4 a 10 pontos/m²*, *pertencentes ao Instituto Geográfico e Cartográfico—IGC, Sistema Cartográfico do Estado de São Paulo*. Acknowledgments are extended to the Editor-in-Chief and the anonymous reviewers for their criticism and suggestions, which helped to improve this paper.

Funding

This research was supported by the São Paulo Research Foundation (FAPESP) grant #2023/11197-1, CNPq #300033/2025-7, #311209/2021-1, CAPES Finance Code-001, CAPES PIPD grant #88887.122984/2025-00.

Conflicts of Interest

The authors declare no conflicts of interest.

Data Availability Statement

The data that support the findings of this study are available in Zenodo at https://doi.org/10.5281/zenodo.16903678 (Coelho, R.D., Frugis, G.L., Viana, C.D., Grohmann, C.H., 2025. High-resolution Digital Terrain Model and Land-surface Parameters of São Sebastião, southeastern Brazil. *Zenodo*. Dataset Version: 1.0) and https://doi.org/10.5281/zenodo.16903853 (Frugis, G.L., Coelho, R.D., Viana, C.D., Grohmann, C.H., 2025. High-resolution Digital Terrain Model and Land-surface Parameters of Ilhabela, southeastern Brazil. *Zenodo*. Dataset Version: 1.0).

Endnotes

[1] https://www.usgs.gov/3d-elevation-program—Last accessed 1 November 2025.

[2] Value calculated using the Digital Index Map (4th edition, 2011), based on the 'available' (*disponíveis*) topographic maps (direct download link).

[3] https://bdgex.eb.mil.br/bdgexapp—Last accessed 1 November 2025.

[4] https://geobases.es.gov.br—Last accessed 1 November 2025.

[5] https://sigsc.sc.gov.br/—Last accessed 1 November 2025.

[6] Accessible via the Brazilian Army BDGEx Portal.

[7] https://sema.portal.ap.gov.br—Last accessed 1 November 2025.

[8] https://pe3d.pe.gov.br/—Last accessed 1 November 2025.

[9] https://geosampa.prefeitura.sp.gov.br/—Last accessed 1 November 2025.

[10] https://www.whiteboxgeo.com/manual/wbt_book/intro.html.

[11] https://www.whiteboxgeo.com/manual/wbw-user-manual/book/preface.html.

[12] http://www.bdg.ibge.gov.br/appbdg/.

[13] https://www.idesp.sp.gov.br/geonetwork/srv/por/catalog.search#/metadata/b295f3cb-9e03-44e6-80db-f929b252418f.

References

Alcântara, E., C. F. Baião, Y. C. Guimarães, J. R. Mantovani, and J. A. Marengo. 2024. "Machine Learning Approaches for Mapping and Predicting Landslide-Prone Areas in São Sebastião (Southeast Brazil)." *Natural Hazards Research* 5: 247–261. https://doi.org/10.1016/j.nhres.2024.10.003.

Aleotti, P., and R. Chowdhury. 1999. "Landslide Hazard Assessment: Summary Review and New Perspectives." *Bulletin of Engineering Geology and the Environment* 58, no. 1: 21–44. https://doi.org/10.1007/s100640050066.

Anderson, E. S., J. A. Thompson, D. A. Crouse, and R. E. Austin. 2006. "Horizontal Resolution and Data Density Effects on Remotely Sensed LIDAR-Based DEM." *Geoderma* 132, no. 3–4: 406–415. https://doi.org/10.1016/j.geoderma.2005.06.004.

ASPRS. 2011. *LAS Specification Version 1.4—R14*. American Society for Photogrammetry and Remote Sensing Accessed July 7, 2025. https://www.asprs.org/wp-content/uploads/2019/03/LAS_1_4_r14.pdf.

ASPRS. 2024. *American Society for Photogrammetry and Remote Sensing (ASPRS) Positional Accuracy Standards for Digital Geospatial Data*. 2nd ed. ASPRS.

Bielski, C., C. López-Vázquez, C. H. Grohmann, et al. 2024. "Novel Approach for Ranking DEMs: Copernicus DEM Improves One Arc Second Open Global Topography." *IEEE Transactions on Geoscience and Remote Sensing* 62: 1–22. https://doi.org/10.1109/TGRS.2024.3368015.

Bonini, J. E., T. D. Martins, M. T. d. O. Sugiyama, and B. C. Vieira. 2025. "Landslide Inventory of the 2023 Serra Do Mar Disaster (Brazil)." *Discover Geoscience* 3, no. 1: 40. https://doi.org/10.1007/s44288-025-00153-2.

Carabajal, C. C., and D. J. Harding. 2006. "SRTM C-Band and ICESat Laser Altimetry Elevation Comparisons as a Function of Tree Cover and Relief." *Photogrammetric Engineering and Remote Sensing* 72, no. 3: 287–298. https://doi.org/10.14358/PERS.72.3.287.

Cirilo, J. A., F. H. B. Alves, L. A. C. Silva, and J. H. A. L. Campos. 2014. "Suporte de informações georreferenciadas de alta resolução para implantação de infraestrutura e planejamento territorial." *Revista Brasileira de Geografia Física* 7, no. 4: 755–763. https://doi.org/10.26848/rbgf.v7.4.p755-763.

Coelho, R. D., C. D. Viana, V. C. Dias, and C. H. Grohmann. 2024. "Landslides of the 2023 Summer Event of São Sebastião, Southeastern Brazil: Spatial Dataset." *Brazilian Journal of Geology* 54, no. 2: e20240006. https://doi.org/10.1590/2317-4889202420240006.

Crippen, R., S. Buckley, P. Agram, et al. 2016. "Nasadem Global Elevation Model: Methods and Progress." In *The International Archives of the Photogrammetry, Remote Sensing and Spatial Information Sciences, XLI-B4*, 125–128. https://doi.org/10.5194/isprs-archives-XLI-B4-125-2016.

Dias, H. C., D. Hölbling, and C. H. Grohmann. 2021. "Landslide Susceptibility Mapping in Brazil: A Review." *Geosciences* 11, no. 10: 425. https://doi.org/10.3390/geosciences11100425.

Dusseau, D., Z. Zobel, and C. R. Schwalm. 2023. "Diluviumdem: Enhanced Accuracy in Global Coastal Digital Elevation Models." *Remote Sensing of Environment* 298: 113812. https://doi.org/10.1016/j.rse.2023.113812.

Farr, T. G., P. A. Rosen, E. Caro, et al. 2007. "The Shuttle Radar Topography Mission." *Reviews of Geophysics* 45: RG2004. https://doi.org/10.1029/2005RG000183.

Florinsky, I. V. 2016. *Digital Terrain Analysis in Soil Science and Geology*. Elsevier.

Florinsky, I. V. 2017. "An Illustrated Introduction to General Geomorphometry." *Progress in Physical Geography: Earth and Environment* 41, no. 6: 723–752. https://doi.org/10.1177/0309133317733667.

Fowler, R., A. Samberg, M. J. Flood, and T. J. Greaves. 2007. *Digital Elevation Model Technologies and Applications: The DEM Users Manual*. 2nd ed, 119–252. Ch. Topographic and Terrestrial Lidar.

Gallant, J. C., and J. P. Wilson. 2000. "Primary Topographic Attributes." In *Terrain Analysis: Principles and Applications*, edited by J. P. Wilson and J. C. Gallant, 51–86. Wiley.

Giraldo-Arroyave, M. I., S. R. F. Vlach, and P. M. Vasconcelos. 2021. "New High-Precision 40 Ar/39 Ar Ages for the Serra Do Mar Alkaline Magmatism in the São Sebastião Island, se Brazil, and Implications." *Brazilian Journal of Geology* 51, no. 4: e20210046. https://doi.org/10.1590/2317-4889202120210046.

Girardeau-Montaut, D. 2019. "Cloudcompare (Version 2.10.3 Zephyrus)." http://www.cloudcompare.org/.

Grohmann, C. H. 2015. "Radiography of the Amazon DSM/DTM Data: Comparative Analysis With SRTM, ASTER GDEM." In: *Geomorphometry 2015*, Poznam, Poland. http://www.geomorphometry.org/Grohmann2015.

Grohmann, C. H., and F. Gomes. 2022. "Digital Terrain and Surface Models of São Paulo." https://doi.org/10.34740/KAGGLE/DS/1915612.

Grohmann, C. H., C. Riccomini, and F. M. Alves. 2007. "SRTM-Based Morphotectonic Analysis of the Poços de Caldas Alkaline Massif, Southeastern Brazil." *Computers & Geosciences* 33, no. 1: 10–19. https://doi.org/10.1016/j.cageo.2006.05.002.

Grohmann, C. H., M. J. Smith, and C. Riccomini. 2011. "Multiscale Analysis of Topographic Surface Roughness in the Midland Valley, Scotland." *IEEE Transactions on Geoscience and Remote Sensing* 49, no. 4: 1200–1213. https://doi.org/10.1109/TGRS.2010.2053546.

Grohmann, C. H., and S. S. Steiner. 2008. "SRTM Resample With Short Distance-Low Nugget Kriging." *International Journal of Geographical Information Science* 22, no. 8: 895–906. https://doi.org/10.1080/13658810701730152.

Guth, P. L., and T. M. Geoffroy. 2021. "LiDAR Point Cloud and ICESat-2 Evaluation of 1 Second Global Digital Elevation Models: Copernicus Wins." *Transactions in GIS* 5: 2245–2261. https://doi.org/10.1111/tgis.12825.

Guth, P. L., S. Trevisani, C. H. Grohmann, et al. 2024. "Ranking of 10 Global One-Arc-Second DEMs Reveals Limitations in Terrain Morphology Representation." *Remote Sensing* 16, no. 17: 3273. https://doi.org/10.3390/rs16173273.

Guth, P. L., A. Van Niekerk, C. H. Grohmann, et al. 2021. "Digital Elevation Models: Terminology and Definitions." *Remote Sensing* 13, no. 18: 3581. https://doi.org/10.3390/rs13183581.

Guzzetti, F., A. C. Mondini, M. Cardinali, F. Fiorucci, M. Santangelo, and K.-T. Chang. 2012. "Landslide Inventory Maps: New Tools for an Old Problem." *Earth-Science Reviews* 112, no. 1–2: 42–66. https://doi.org/10.1016/j.earscirev.2012.02.001.

Hawker, L., P. Uhe, L. Paulo, et al. 2022. "A 30 m Global Map of Elevation With Forests and Buildings Removed." *Environmental Research Letters* 17, no. 2: 024016. https://doi.org/10.1088/1748-9326/ac4d4f.

Hengl, T. 2006. "Finding the Right Pixel Size." *Computers and Geosciences* 32, no. 9: 1283–1298. https://doi.org/10.1016/j.cageo.2005.11.008.

Ho, Y.-F., C. H. Grohmann, J. Lindsay, et al. 2025. "GEDTM30: Global Ensemble Digital Terrain Model at 30 m and Derived Multiscale Terrain Variables." *PeerJ* 13: e19673. https://doi.org/10.7717/peerj.19673.

Horn, B. K. P. 1981. "Hill Shading and the Reflectance Map." *Proceedings of the IEEE* 69, no. 1: 14–47. https://doi.org/10.1109/PROC.1981.11918.

IBGE. 2023. *Modelo hgeoHNOR2020 para conversão de altitudes geométricas em altitudes normais*. 2nd ed. Volume 47 of Relatórios Metodológicos. Instituto Brasileiro de Geografia e Estatística Available Only as Digital Media. https://biblioteca.ibge.gov.br/index.php/biblioteca-catalogo?view=detalhesid=2102048.

Imhof, E. 1982. *Cartographic Relief Presentation*. Walter de Gruyter.

Infraestrutura de Dados Espaciais do Estado de São Paulo. 2023. "Vôo 2023 São Sebastião 10 cm Vila Sahy." *São Paulo*. Accessed November 1, 2025. https://www.idesp.sp.gov.br/geonetwork/srv/por/catalog.search#/metadata/%7B4A9B4AB9-BBD9-4D6B-8D9D-BFBD679B8042%7D.

Jasiewicz, J., and T. F. Stepinski. 2013. "Geomorphons—A Pattern Recognition Approach to Classification and Mapping of Landforms." *Geomorphology* 182: 147–156. https://doi.org/10.1016/j.geomorph.2012.11.005.

Koenderink, J. J., and A. J. van Doorn. 1992. "Surface Shape and Curvature Scales." *Image and Vision Computing* 10, no. 8: 557–564. https://doi.org/10.1016/0262-8856(92)90076-f.

Laipelt, L., B. de Comini Andra, W. Collischonn, A. de Amorim Teixeira, R. C. D. Paiva, and A. Ruhoff. 2024. "ANADEM: A Digital Terrain Model for South America." *Remote Sensing* 16, no. 13: 2321. https://doi.org/10.3390/rs16132321.

Lindsay, J. 2016. "Whitebox GAT: A Case Study in Geomorphometric Analysis." *Computers & Geosciences* 95: 75–84. https://doi.org/10.1016/j.cageo.2016.07.003.

Lindsay, J. B. 2018. "A New Method for the Removal of Off-Terrain Objects From LiDAR-Derived Raster Surface Models." https://www.researchgate.net/publication/323003064_A_new_method_for_the_removal_of_off-terrain_objects_from_LiDAR-derived_raster_surface_models.

Lindsay, J. B., and K. Dhun. 2015. "Modelling Surface Drainage Patterns in Altered Landscapes Using Lidar." *International Journal of Geographical Information Science* 29, no. 3: 397–411. https://doi.org/10.1080/13658816.2014.975715.

Lindsay, J. B., A. Francioni, and J. M. H. Cockburn. 2019. "LiDAR DEM Smoothing and the Preservation of Drainage Features." *Remote Sensing* 11, no. 16: 1926. https://doi.org/10.3390/rs11161926.

Lindsay, J. B., D. R. Newman, and A. Francioni. 2019. "Scale-Optimized Surface Roughness for Topographic Analysis." *Geosciences* 9, no. 7: 322. https://doi.org/10.3390/geosciences9070322.

Marengo, J. A., A. P. Cunha, M. E. Seluchi, et al. 2024. "Heavy Rains and Hydrogeological Disasters on February 18th–19th, 2023, in the City of São Sebastião, São Paulo, Brazil: From Meteorological Causes to Early Warnings." *Natural Hazards* 120, no. 8: 7997–8024. https://doi.org/10.1007/s11069-024-06558-5.

Mark, D. M., and B. Smith. 2004. "A Science of Topography: From Qualitative Ontology to Digital Representations." In *Geographical Information Science and Mountain Geomorphology*, edited by M. P. Bishop and J. F. Shroder, 75–100. Springer-Praxis.

Nelson, A., H. I. Reuter, and P. Gessler. 2009. "Chapter 3: DEM Production Methods and Sources." In *Geomorphometry: Concepts, Software, Applications. Volume 33 of Developments in Soil Science*, edited by T. Hengl and H. I. Reuter, 65–85. Elsevier. https://doi.org/10.1016/S0166-2481(08)00003-2.

O'Callaghan, J. F., and D. M. Mark. 1984. "The Extraction of Drainage Networks From Digital Elevation Data." *Computer Vision, Graphics, and Image Processing* 28, no. 3: 323–344. https://doi.org/10.1016/S0734-189X(84)80011-0.

Organisation for Economic Co-Operation and Development. 2015. "Making Open Science a Reality." https://doi.org/10.1787/5jrs2f963zs1-en.

Pike, R. J., I. S. Evans, and T. Hengl. 2009. "Chapter 1. Geomorphometry: A Brief Guide." In *Geomorphometry: Concepts, Software, Applications*, edited by T. Hengl and H. I. Reuter, 3–30. Elsevier. https://doi.org/10.1016/S0166-2481(08)00001-9.

Pronk, M., A. Hooijer, D. Eilander, et al. 2024. "Deltadtm: A Global Coastal Digital Terrain Model." *Scientific Data* 11: 273. https://doi.org/10.1038/s41597-024-03091-9.

Qin, C., A. Zhu, T. Pei, B. Li, C. Zhou, and L. Yang. 2007. "An Adaptive Approach to Selecting a Flow-Partition Exponent for a Multiple-Flow-Direction Algorithm." *International Journal of Geographical Information Science* 21, no. 4: 443–458. https://doi.org/10.1080/13658810601073240.

Sato, E., S. Vlach, and M. Basei. 2008. *Zircon and Baddeleyite U-Pb Dating (TIMS) of Mesozoic Alkaline Rocks From the São Sebastião Island, Southeastern Brazil*. International Geological Congress. https://repositorio.usp.br/item/001717959.

Sato, E. N. 2006. "Petrografia e Geocronologia U/Pb (tims) de rochas alcalinas da ilha de são sebastião (sp)." Ph.D. thesis, Universidade de São Paulo. https://bdta.abcd.usp.br/item/001662223.

Strobl, P. 2020. "The New Copernicus Digital Elevation Model." *GSICS Quarterly* 14, no. 1: 11–14. https://doi.org/10.25923/enp8-6w06.

Strobl, P. A., C. Bielski, P. L. Guth, et al. 2021. "The Digital Elevation Model Intercomparison eXperiment DEMIX, a Community Based Approach at Global DEM Benchmarking." In *The International Archives of the Photogrammetry, Remote Sensing and Spatial Information Sciences*, XLIII-B4-2021, 395–400. https://doi.org/10.5194/isprs-archives-XLIII-B4-2021-395-2021.

Tachikawa, T., M. Hato, M. Kaku, and A. Iwasaki. 2011. "Characteristics of ASTER GDEM Version 2." In *2011 IEEE International Geoscience and Remote Sensing Symposium (IGARSS)*, 3657–3660. https://doi.org/10.1109/IGARSS.2011.6050017.

Tadono, T., J. Takaku, K. Tsutsui, F. Oda, and H. Nagai. 2015. "Status of ALOS World 3D (AW3D) Global DSM Generation." In *2015 IEEE International Geoscience and Remote Sensing Symposium (IGARSS)*, 3822–3825. https://doi.org/10.1109/IGARSS.2015.7326657.

Tedersoo, L., R. Küngas, E. Oras, et al. 2021. "Data Sharing Practices and Data Availability Upon Request Differ Across Scientific Disciplines." *Scientific Data* 8, no. 1: 192. https://doi.org/10.1038/s41597-021-00981-0.

Uhe, P., C. Lucas, L. Hawker, et al. 2025. "Fathomdem: An Improved Global Terrain Map Using a Hybrid Vision Transformer Model." *Environmental Research Letters* 20, no. 3: 034002. https://doi.org/10.1088/1748-9326/ada972.

Valeriano, M. M., T. M. Kuplich, M. Storino, B. D. Amaral, J. N. Mendes, and D. J. Lima. 2006. "Modeling Small Watersheds in Brazilian Amazonia With Shuttle Radar Topographic Mission-90m Data." *Computers & Geosciences* 32: 1169–1181. https://doi.org/10.1016/j.cageo.2005.10.019.

Varnier, M. 2024. "A Cloud-Based and Open-Source Approach to Generate Landslide Susceptibility Maps." *Revista Brasileira de Geomorfologia* 25, no. 2: e2491. https://doi.org/10.20502/rbgeomorfologia.v25i2.2491.

Winsen, M., and G. Hamilton. 2023. "A Comparison of UAV-Derived Dense Point Clouds Using LiDAR and NIR Photogrammetry in an Australian Eucalypt Forest." *Remote Sensing* 15, no. 6: 1694. https://doi.org/10.3390/rs15061694.

Supporting Information

Additional supporting information can be found online in the Supporting Information section. **Data S1:** gdj370057-sup-0001-Supinfo.csv.